COLLOQUE DE PHYSIQUE
Colloque C7, supplément au n°23, Tome 51, 1er décembre 1990

SHAPE TRANFORMATIONS OF FREE, TOROIDAL AND BOUND VESICLES

U. SEIFERT[1]

Sektion Physik, Universität München, Theresienstrasse 37, D-8000 München 2, F.R.G.

ABSTRACT - Shapes and shape transformations of vesicles are considered theoretically within the spontaneous curvature model for three cases. (i) For free vesicles, the whole phase diagram is presented which includes pear-shaped vesicles and a line of limit shapes related to budding. (ii) For toroidal vesicles, three branches of solutions with low energy are found. (iii) An extension of this model to the adhesion of vesicles is briefly discussed.

I. INTRODUCTION

Vesicles are closed surfaces of lipid bilayer which form spontaneouosly in aequous solutions in order to prevent contact between the hydrocarbon chains and the water.[1] They exhibit a wide variety of different shapes including biconcave discocytes and cup-shaped stomatocytes. Transformations between these shapes can be induced ,*e.g.*, by changing the temperature.[2] Recently, the phenomenon of budding, *i.e.*, the expulsion of a small vesicle has attracted much interest.[3] The theoretical description of shape transformations is based on the concept of bending elasticity for which a curvature model is considered. In this model, the vesicle is described as a two dimensional surface embedded in three dimensional space. In the version introduced by Helfrich, the bending elasticity is expressed by[4,5]

$$F_b \equiv F_\kappa + F_{\kappa_G} \equiv (\kappa/2) \oint dA(C_1 + C_2 - C_0)^2 + \kappa_G \oint dA\, C_1 C_2. \qquad (1)$$

The variables C_1 and C_2 denote the two principal curvatures, while the spontaneous curvature C_0 is a phenomenological parameter introduced in order to account for a possible asymmetry of the bilayer. κ and κ_G denote the two bending rigidities.

A second version of the curvature model is the bilayer coupling model.[6,7] Here it is assumed that the two monolayers do not exchange area on experimentally relevant time-scales which leads to a constraint on the integrated mean curvature, $(1/2) \oint dA(C_1 + C_2)$. Both models are then related via a Legendre transformation.

In this paper, I will discuss recent theoretical progress for the spontaneous curvature model. In Sect.II, the phase diagram is presented for vesicles of spherical topology. These results are part of a systematic study of the phase diagram for both variants of the curvature model and will be discussed in more detail elsewhere (U. Seifert, K. Berndl and R. Lipowsky, to be published). In Sect.III, the possibility of shapes with the topology of a torus is investigated. Finally, I briefly discuss the basic features of an extension of the model (1) to the adhesion of vesicles in Sect.IV.

II. PHASE DIAGRAM FOR VESICLES OF SPHERICAL TOPOLOGY

The phase diagram is determined by the shape of lowest bending energy for given area A and enclosed volume V. These constraints are introduced with Lagrange multipliers Σ and P. The shape equations then derive from

$$\delta F \equiv \delta(F_b + \Sigma A + PV) = 0, \qquad (2)$$

where δ denotes variation with respect to the shape of the vesicle and Σ and P are adjusted in order to guarantee the prescribed area and volume. The Gaussian curvature term, F_{κ_G}, is a topological invariant given by $F_{\kappa_G} = 4\pi\kappa_G(1-g) = 2\pi\chi$, where g denotes the number of holes or the genus of the vesicle and χ its Euler characteristics. Therefore, it does not show up in the shape equation. In general, (2) is a partial differential equation of fourth order.[8] For axi-symmetric shapes, the shape equation reduces to four (or six, if the constraints are already imposed) coupled nonlinear differential equations which can be solved on a computer. Because of the scale invariance of the bending energy,

(1) Address past October 1st: Department of Physics, Simon Fraser University, Burnaby, B.C., V5A1S6, Canada

it is sufficient to discuss the solutions to this equation as a function of the two reduced variables v and c_0, with

$$v \equiv V/\{(4\pi/3)[A/(4\pi)]^{3/2}\} \quad \text{and} \quad c_0 \equiv C_0(A/4\pi)^{1/2}. \tag{3}$$

For nearly spherial vesicles with $v \approx 1$, the solutions of the shape equations can be classified according to branches which result from deformations of a sphere with spherical harmonics $Y^{l,m}$. Since it is known that shapes which correspond to $l \geq 3$ are locally unstable,[9] the physically relevant solutions are those with $l = 2$, *i.e.,* the prolate and oblate ellipsoids.

First, consider the prolate ellipsoids and the shapes which evolve along this branch when the volume is reduced. For $c_0 = 0$, the prolate shapes become then dumbbell-like and finally approch a long thin cylinder. With increasing c_0, this prolate branch develops additional structure. As an illustrative example consider Fig.1, where the bending energy and the corresponding shapes are displayed as a function of the reduced volume for $c_0 = 2.4$. The prolate branch now consists of two parts (prolate-1 and prolate-2), which are connected by asymmetric pear-shaped vesicles.(1) The pear-shaped branch bifurcates from both parts of the symmetric branch and consists of two parts which meet in the point of maximal volume. It is evident from the bifurcation diagram that the upper part of the pear-shaped branch corresponds to shapes which are locally unstable with respect to axi-symmetric deformations. The unstable mode drives these shapes either back to the symmetric shapes or to the asymmetric shapes with the narrow neck which lie on the lower part of the pear-shaped branch. Of course, stability with respect to non-axisymmetric deformations can not be read off from such an energy diagram.

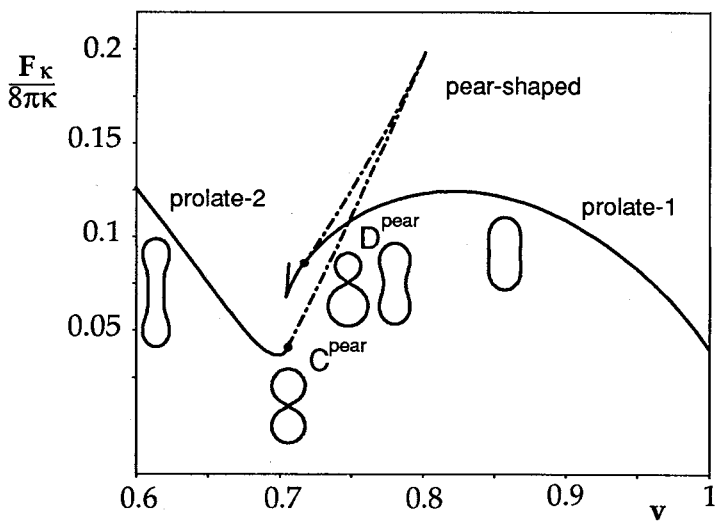

FIG.1: Bending energy and shapes of lowest energy for $c_0 = 2.4$. The two prolate branches are connected by a branch of asymmetric pear-shaped vesicles. This leads to a discontinuous transition D^{pear} between the prolate-1 and the pear-shaped states and to an continuous transition C^{pear} between the pear-shaped and the prolate-2 states.

With decreasing volume, a spherical vesicle becomes, thus, first prolate and then metastable beyond D^{pear} where a discontinuous transition to the asymmetric shapes occurs. These shapes become continuously symmetric again at C^{pear} and finally approach a long cylinder for $v \to 0$.

Analysis of the c_0-dependence of these transitions leads to the phase diagram as displayed in Fig.2. For $2.08 \lesssim c_0 < 2\sqrt{2}$, the sequence of shape transformations proceeds as just described. For

(1) These shapes have independently been found by Wiese and Helfrich[10], Svetina, Kralj-Iglic and Zeks (preprint) and the group of M. Wortis (private communication).

$2.066 \lesssim c_0 \lesssim 2.08$, there is a discontinuous transition D^{pro} between two different prolate shapes. For $c_0 \lesssim 2.066$, only one type of symmetric prolate shape gives the state of lowest energy.

For $c_0 > 2\sqrt{2}$, a new phenomenon happens. The branch of pear-shaped vesicles terminates in a *limit shape* L^{pear} where an infinitesimal neck connects two spheres of different radii R_1 and R_2. Such an *ideal neck* nevertheless does not cost energy, since the two curvatures of the neck have compensating signs. The locus of this limit shape is determined by

$$C^A + C^B = C_0, \tag{4}$$

which relates the two inverse radii $C^A = 1/R_1$ and $C^B = 1/R_2$ of the limit shape to the spontaneous curvature. If R_1 and R_2 are expressed by the area and the volume, an analytic expression $v(c_0)$ for the line L^{pear} of limit shapes can be derived. This line corresponds to the end points of *budding trajectories* in the spontaneous curvature model. The value $c_0 = 2\sqrt{2}$ is the smallest value of c_0 for which budding occurs. At this point, both spheres have the same radius. The larger c_0 is, the smaller is the radius of the expelled vesicle. For $c_0 \to \infty$, the phase boundary D^{pear} and the line of limit shapes L^{pear} approach $v = 1$.

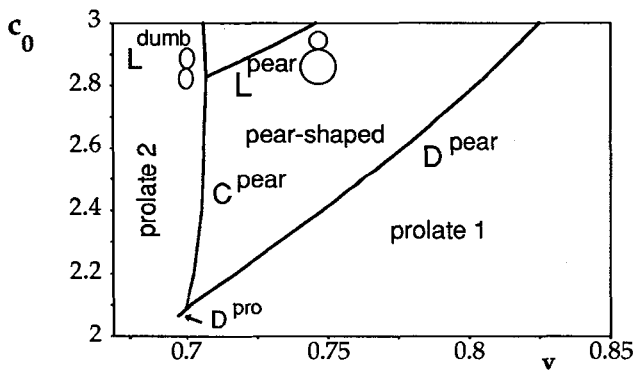

FIG.2: Phase diagram of the spontaneous curvature model in the region where the pear-shaped vesicles arise. D^{pear} and D^{pro} denote discontinuous transitions, C^{pear} denotes a continuous transition. L^{pear} and L^{dumb} denote limit lines.

Similarly for the dumbbell-like shapes of the second symmetric branch, prolate-2, an increase in v leads to a limit shape L^{dumb} where two identical prolate shapes are connected by an ideal neck. Again, the relation (4) holds where $C^A = C_1^A = C_2^A$ and $C^B = C_1^B = C_2^B$ denote the *local* curvature at the poles of the two adjacent prolates. The relation (4) is rather universal since we have found several limit shapes which consist of two or even more parts which are connected by ideal necks obeying (4).

Now, consider the oblate ellipsoids. With decreasing volume, they become biconcave discocytes. In the c_0-range just described, shapes of the oblate/discocyte branch have larger energy than the prolate and pear-shaped vesicles. Therefore, they do not show up in the region of the phase diagram displayed in Fig.2. For lower values of the spontaneous curvature, however, there is a discontinuous transition from prolates to oblates as displayed in the phase diagram Fig.3. The oblate/discocyte shapes then undergo a second discontinuous transition to the stomatocytes which terminate at limit shapes where a small inverted sphere of radius $R_1 < 0$ is embedded in a larger sphere of radius R_2. The loci of these limit shapes are once more determined by relation (4), with $C^A = 1/R_1$ and $C^B = 1/R_2$. The oblate/discocyte and the stomatocyte region are moreover bounded by lines which denote the selfintersection of the shapes at the two poles. For the oblate/discocytes, this line is related to the occurence of toroidal vesicles as discussed below.

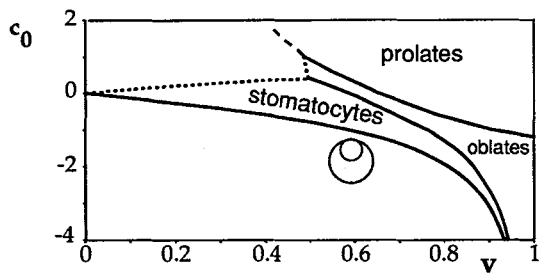

FIG.3: Phase diagram for $c_0 < 2$. The prolate, oblate and stomatocyte regions are separated by discontinous transitions. The stomatocyte region is also bounded by a line of limit shapes where a sphere includes a spherical cavity. The dotted lines denote selfintersection of the oblate and stomatocyte vesicles which define the physical limit of the model. The dashed line is the continuation of the prolate-oblate transition into this region of selfintersection.

This detailed investigation of the phase diagram provides the basis for a crucial experimental test of model (1) provided it is known how v and c_0 vary with experimentally controllable parameters. Consider, *e.g.,* an increase in temperature. This leads via (3) to a decrease in v since the area expansivity of the bilayer is significantly larger than the volume expansivity of the enclosed water. Although the temperature dependence of c_0 is not obvious, any trajectory starting near the sphere which ends either at the budding line or at the limit shapes for the stomatocytes, must pass through at least one discontinuous transition before that limit shape is reached. This is in contrast with the predictions of the bilayer coupling model for which the oblate-stomatocyte as well as the prolate-pear-shaped transition is continuous. Based on such an analysis for both models, we reached good agreement with a recent experiment using the bilayer coupling model and assuming a small asymmetry in the monolayer expansivities. (K. Berndl, J. Käs, R. Lipowsky, E. Sackmann and U. Seifert, submitted for publication.) More experiments on different systems are certainly required to obtain a complete picture.

III. SHAPES OF TOROIDAL TOPOLOGY

Although vesicle shapes of toroidal topology have not been reported so far, there is no fundamental reason against their occurrence. In fact, it turns out that already for $c_0 = 0$ they have a lower energy F_κ than the vesicles of spherical topology for a large range of v-values. Of course, for the total bending energy also the difference in Gaussian curvature energy must be considered which is given by the value of the sphere $4\pi\kappa_G$ since the Euler characteristic of a torus vanishes. Therefore, a positive value of κ_G should favour toroidal vesicles.

The shape equations (2) remain valid for the toroidal topology which must be enforced by appropriate boundary conditions. As a result, I find three branches of axi-symmetric toroidal shapes which can be characterized according to a typical cross-section as (i) the *circular* toroids (Fig.4a), (ii) the *sickle-shaped* toroids (Fig.4b), and (iii) the *discoid* toroids (Fig.4c).

In Fig.5, the bending energy F_κ is displayed as a function of v. For comparison, the same quantity for the oblate/discocyte branch of spherical topology is also displayed.

The *circular* toroids exist for any $0 < v < 1$. The cross-section of the shapes of this branch is a circle for $v = 3/(2\sqrt{\pi})$ and for $v \to 0$. In this limit, the distance of the cross-section from the axis of symmetry diverges and F_κ diverges as $1/v^2$. For $v = 3/(2\sqrt[5/4]{\pi}) \simeq 0.71$, the two generating radii have the ratio $\sqrt{2}$ and the bending energy acquires its minimum along this branch with $F_\kappa = 4\pi^2\kappa$. This special solution has been previously found analytically.[11](1) For $v > 3/(2\sqrt{\pi})$, F_κ increases again along this branch and for $v \to 1$ the shape seems to approach a sphere excluding an infinitesimal cylinder surrounding the axis of symmetry.

(1) In Ref.11, it is however argued that this special solution is unstable with respect to *axisymmetric* deformations for $C_0(A/4\pi)^{1/2} > c_0^*$, with $c_0^* \simeq -3.9$. Since this toroid has the minimal bending energy of all toroids, it is hard to see to which shape the unstable mode should drive this circular toroid. In addition, I could not find any bifurcation along this whole branch. Therefore, I believe that the circular toroids are locally stable with respect to axi-symmetric deformations for all values of v.

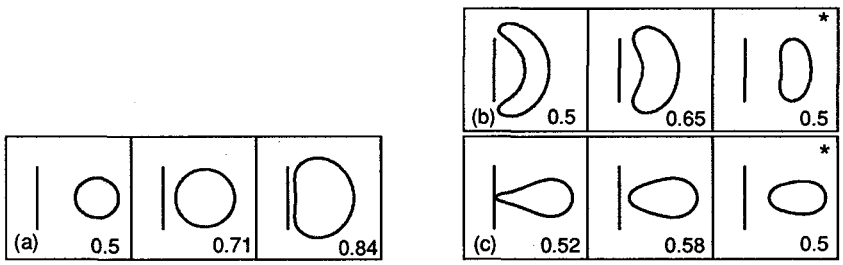

FIG.4: Shapes of toroidal vesicles for several values of the reduced volume v. The bar shows the axis of symmetry. (a) circular toroids; (b) sickle-shaped toroids; (c) discoid toroids. The asterisks denote locally unstable shapes corresponding to the upper parts of the two latter branches, respectively.

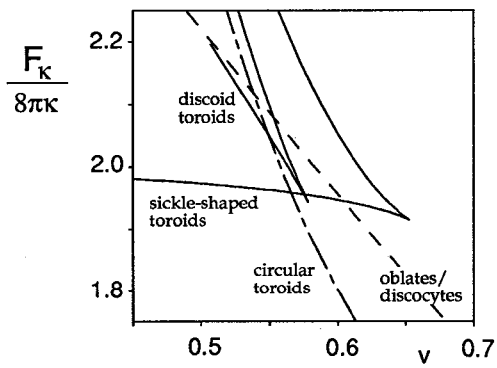

FIG.5: Curvature energy of the three toroidal branches and the oblate/discocyte branch of spherical topology.

The branch of *sickle-shaped* toroids consists of two parts which are connected at a point of maximal volume. As discussed in Sect.II., the upper part of such cusped branches can be identified with solutions which are locally unstable, while the lower part corresponds to shapes which are locally stable, at least with respect to axi-symmetric deformations. For $v \to 0$, the stable part approaches a limit shape, which consists of an inverted sphere embedded in a sphere with the same radius. Both spheres are connected by two ideal necks. Consequently, F_κ approaches the value $16\pi\kappa$ of two spheres in this limit. For $v > 0$, the energy of these sickle-shaped toroids decreases monotoneously and reaches its minimum for maximal volume.

The *discoid* branch also consists of two parts. The lower, locally stable part exists for $0.50 \lesssim v \lesssim 0.58$. For $v \to 0.50$, the diameter of the hole goes to zero and the shape approaches - apart from this hole - the shape of a discocyte vesicle of spherical topology where the north and the south pole touch each other. The curvature energy of this toroidal vesicle approaches the mean curvature energy, F_κ of the discocyte vesicle from below.

This merging of branches with different topology should facilitate the formation of toroidal vesicles. Suppose that a discocyte vesicle of spherical topology is driven into this v-range, *e.g.*, by increasing the temperature. If the hole formation can be enforced externally, ([1]) the toroidal vesicle should remain stable provided $\kappa_G > 0$. Therefore such an experiment could yield the sign of the Gaussian bending rigidity. Once this discoid toroid has been created, fascinating experiments should be possible. Since this toroid has larger energy than the sickle-shaped toroids over a large range of v-values, it should

([1]) A possible technique could be electroporation[12] or photodissociation of special amphiphiles imbedded in the membrane. The latter method was successful in transforming a necklace of vesicles into single separated vesicles.[13]

undergo a transition to the latter state. The sickle-shaped vesicle, finally, must transform to a circular toroid for increasing v. This sequence of shape transformations can be read off from Fig.5.

A global comparison of the curvature energy of shapes of spherical and toroidal topology reveals that that the state of lowest bending energy for $\kappa_G = 0$ is a sickle-shaped toroid for $0 < v \lesssim 0.56$, a circular toroid for $0.56 \lesssim v \lesssim 0.73$ and a prolate shape for $0.73 \lesssim v \lesssim 1$. For $\kappa_G \neq 0$, the relative position of the two families of different topology is shifted by $4\pi\kappa_G$ which is the difference in Gaussian curvature energy.

IV. ADHESION OF VESICLES

The adhesion of giant vesicles has been investigated by micro-pipet techniques[14] while accidental adhesion of membranes in dilute systems can be studied with light microscopy[15]. Theoretically, adhesion of vesicles can be discussed by an extension of model (1).[16–18] A vesicle bound to a 'wall', which might be another membrane or a substrate gains the adhesion energy

$$F_W = -WA^*, \tag{5}$$

where A^* denotes the contact area of the vesicle with the wall and W denotes the strength of the adhesion potential. Bound vesicle states and the phase diagram are now determined by the minimum of $F_\kappa + F_W$. This minimization leads to a universal boundary condition for the contact curvature C_1^*,

$$C_1^* = \sqrt{2W/\kappa}, \tag{6}$$

at the point where the vesicles contour meets the wall.[16] Of course, the contour meets the wall tangentially since any other contact angle would imply an infinite bending energy. Solutions of the shape equation (2) with the boundary condition (6) lead to a similar variety of bound vesicle shapes as for free vesicles. Likewise, shape transitions between different bound states occur. As a novel feature, the competition between bending and adhesion energy leads to an adhesion transition. For $W < 4\pi w_a(v)\kappa/A$, where $w_a(v)$ is of order unity and depends only on v (and c_0), the vesicles are free even in the presence of an attractive wall.[16,17] For fixed potential strength W, the scale dependence of the adhesion transition thus leads to a lower cutoff for the size of bound vesicle states. For a bound vesicle, an increase in W leads to a shape which approaches a spherical cap. In this limit, an *effective* contact angle Ψ_{eff} can be defined which relates the tension Σ, as given by the Lagrange multiplier, and the wall potential W by a Young-Dupré equation $W = \Sigma(1+\cos\Psi_{eff})$. Strong adhesion, however, will also induce topological changes like fusion and the rupture of bound vesicles.[18]

ACKNOWLEDGEMENT

I thank K. Berndl, J. Käs, R. Lipowsky and E. Sackmann for enjoyable collaboration. Stimulating discussions with E. Evans, B. Fourcade, W. Helfrich, M. Peterson and M. Wortis are greatfully acknowledged. Finally, I thank J. Krug for a critical reading of the manuscript. This work was supported by the Deutsche Forschungsgemeinschaft via SFB 266.

REFERENCES

1. See, *e.g., Physics of Amphiphilic Layers*, ed. by J. Meunier, D. Langevin, and N. Boccara, Springer Proc. in Physics, Vol. 21 (Springer, Berlin, 1987).
2. E. Sackmann, H.P. Duwe and H. Engelhardt, *Farad. Discuss. Chem. Soc.* **81**, 281 (1986).
3. E. Evans and W. Rawicz, *Phys. Rev. Lett.* **64**, 2094 (1990).
4. W. Helfrich, *Z. Naturforsch.* **28c**, 693 (1973).
5. H.J. Deuling and W. Helfrich, *J. Phys. France* **37**, 1335 (1976).
6. S. Svetina and B. Zeks, *Biomed. Biochim. Acta* **42**, 86 (1983).
7. S. Svetina and B. Zeks, *Eur. Biophys. J.* **17**, 101 (1989).
8. Ou-Yang Zhong-can and W. Helfrich, *Phys. Rev. Lett.* **59**, 2486 (1987).
9. M.A. Peterson, *Phys. Rev. A* **39**, 2643 (1989).
10. W. Wiese and W. Helfrich *J. Phys. Cond. Matter*, in press.
11. Ou-Yang Zhong-can, *Phys. Rev. A* **41**, 4517 (1990).
12. See, *e.g.,* D.C. Chang, *Biophys. J.* **56**, 641 (1989).
13. H.P. Duwe, P. Eggl and E. Sackmann, *Angew. Makromol. Chemie* **166,167** 1 (1989).
14. E. Evans, *Colloids and Surfaces* **43** , 327 (1990).
15. R.M. Servuss and W. Helfrich, *J. Phys. France* **50**, 809 (1989).
16. U. Seifert and R. Lipowsky, *Phys. Rev. A*, (in press).
17. R. Lipowsky and U. Seifert, in *Fluctuations in Lamellae and Membranes*, ACS Symposium Series, Eds. W.J. Benton and L.A. Turkevich, (in press).
18. R. Lipowsky and U. Seifert, *Mol.Cryst.Liq.Cryst.*, (in press).